Marine Structures 81 (2022) 103120

Contents lists available at ScienceDirect

Marine Structures

journal homepage: www.elsevier.com/locate/marstruc

Underwater wet welding of S1300 ultra-high strength steel

Jacek Tomków *, Michał Landowski, Dariusz Fydrych, Grzegorz Rogalski

Faculty of Mechanical Engineering and Ship Technology, Gdańsk University of Technology, Gdańsk, Poland

ARTICLE INFO

Keywords:
Ultra-high strength steel
Underwater welding
Temper bead welding
Weldability
Water environment
Microstructural changes

ABSTRACT

An expected tendency in marine and offshore structures is an increasing share of steels with high mechanical properties. The necessity to perform the welding work under water leads to a decreasing of the weldability of the steel. It results from the increased susceptibility to form cold cracks, especially in welded structures made of high-strength steel. A potential method, which may improve the problem of limited weldability of steel under water is the use of temper bead welding (TBW) technique. In this paper, the possibility of underwater wet welding by covered electrode S1300 ultra-high strength steel of different thickness (4 mm and 10 mm) has been investigated. The visual, metallographic macro- and microscopic tests, and Vickers HV10 measurements of samples with two nonparallel beads were performed. On the basis of the performed tests, the effectiveness of TBW technique was quantitatively verified. It was proved that TBW leads to positive microstructural changes and reduces the number of cracks in different regions of welded joints. Moreover, it was found that the proposed technique allows to decrease the hardness of S1300 steel joint by 30–80 HV10 in the weld metal and 40–100 HV10 in heat-affected zone. Finally, it was stated that the thickness of the base material does not affect the effectiveness of the TBW technique.

1. Introduction

The welding processes are classified as special processes, which have to be controlled in each step of its preparation and realization [1,2]. It is especially important to control the thermal history of the joints. In the case of welding of high-strength low-alloy (HSLA) steel, the most unfavorable is the influence of the short thermal cycles. Short cycles may result from welding of materials of high thickness, the use of low values of heat input, as well as the impact of the environment [3–5]. Among the environmental effects, the most important are welding in low temperature [6], under oil welding [7] and underwater welding [8].

Except the wet welding process carried out directly in the water [9], the local cavity welding [10–12] and dry welding [13,14] are classified as underwater welding methods. The processes most commonly used in wet conditions are flux-cored arc welding (FCAW) [15,16] and manual metal arc welding (MMA) [17]. In the case of FCAW, there are problems with the use of this process in real welding conditions. During the process, the welding arc is surrounded by water vapor, which results in the instability of the process [18], the same as the water pressure [19]. Furthermore, the water environment leads to decreasing the corrosion resistance of welded materials [20]. Another problem occurred during underwater welding is the hydrogen produced by water dissociation near the arc [21]. Water as a welding environment generates almost two times higher values of diffusible hydrogen content in deposited metal for rutile covered

* Corresponding author. G. Narutowicza 11/12 street, 80-233, Gdańsk, Poland.
E-mail addresses: jacek.tomkow@pg.edu.pl (J. Tomków), michal.landowski@pg.edu.pl (M. Landowski), dariusz.fydrych@pg.edu.pl (D. Fydrych), grzegorz.rogalski@pg.edu.pl (G. Rogalski).

https://doi.org/10.1016/j.marstruc.2021.103120
Received 23 June 2021; Received in revised form 25 September 2021; Accepted 3 November 2021

electrodes than during welding in the air [22,23]. It significantly decreases the quality of underwater welded joints. Klett et al. [24] proved a reduction of hydrogen amount with increasing welding depth. A directly proportional relationship between the hydrogenation of the weld metal and the heat input value was also found. As a method of reducing of hydrogen amount, apart from welding polarity and changes in the values of welding parameters [25], electrode sharpening and modification of the electrode covering with additives and a waterproof coating can be used [26]. Moreover, Tomków et al. [18] proposed a modification of filler materials. It was stated that the application of paraffin wax on the covered electrode surface significantly reduces the hydrogen content in the deposited metal. Another positive effect of the use of paraffin wax was the reduction of the number of cracks in heat-affected zone (HAZ). The research results presented so far show that the diffusible hydrogen amount resulted from complex interactions between oxygen content, welding pool volume and cooling rate of weldment [18,19,21,24]. Water as an environment of welding causes high cooling rate of joints. In combination with the critical amount of hydrogen and residual stress, it may cause the phenomenon of cold cracking [27] of joints made of steel with higher hardenability [28]. The susceptibility of steel to cold cracking depends on all factors affecting the three basic conditions causing this phenomenon: brittle structure, diffusible hydrogen, and residual stress and is very difficult to clearly describe and predict. Many investigations showed that the susceptibility to cold cracking may decrease the HSLA steel weldability [29,30]. Tomków et al. [31] determined that cold cracks in HSLA steel are located in the HAZ parallel to the fusion line.

Previous investigations showed that temper bead welding (TBW) is an effective method of reduction tendency of HSLA steel welded under water to cold cracking [27,31]. This involves the use of arc welding as a heat source for the heat treatment of the previously welded layers, by laying successive weld beads. The TBW allows to reduce the grain size, minimalize the value of residual stress, and causes the intensification of hydrogen diffusion to the environment. The favorable role of TBW consists in the simultaneous beneficial effect of all three factors causing the cold cracking of steel welded joints.

The literature analysis showed that the tests of weldability of steels in water environment have been limited to grades of materials classified as HSLA steels. However, novel applications in the marine and offshore industry are increasingly focusing on steels with higher mechanical properties, such as ultra-high strength steels (UHSS) [32,33]. It allows to reduce the weight and dimensions of the structures, without decreasing their load capacity. However, the joining of UHSS still causes problems. Ning et al. [34] stated that the welding process could produce brittle structures in the HAZ, which leads to decreasing the ductility of the performed joints. The next problem occurring in wet welded joints is their relatively short fatigue life, which resulted from formation the welding imperfection during process [35]. Fatigue strength of welded joints is independent of parent material strength in as-welded state [36]. One of the methods, which is used to improve the fatigue strength of UHSS is hammer peening, which was investigated by Berg et al. [37]. The fatigue performance of the welded joints could be improved by machining [38] and grinding [39] of the weld toe. Grinding is one of the most widely used methods of improving the fatigue strength of UHSS [40]. Braun et al. [41] stated that grinding may be applicable to butt- and fillet-welded joints with similar effectiveness.

The water environment significantly impedes the use of these methods in marine conditions. Another problem generated during welding of UHSS is cracking. Schaupp et al. [42] stated that S960 steel is susceptible to hydrogen-assisted cracking. The sensitivity to cold cracking of UHSS steels were proved for similar S1100 [43,44] quenched and tempered steel grades [45].

The mentioned issues suggest that UHSS may be susceptible to cold cracking in underwater wet welding conditions, due to the intensification of the adverse factors during process. To the best of the authors knowledge, there are not any published works in the field of underwater welding of steel with grade above S1000. The necessity to take up the topic arises from the use of UHSS for offshore structures such as wind turbines [46], platforms [47], jack-up structures [48], pipelines [49] and to some extend tubular joints [36]. These structures may undergo failures, which require repairs in the water. The limited weldability of S1300Q steel in the air environment is resulted from the complex chemical composition and specific heat treatment during the manufacturing process. During welding, the multi-phase structure of steel is subjected by the influence of simple, and in the case of elements of greater thickness, multiple thermal cycles. It determines the properties of welded joints. Depending on the factors determining the thermal severity: welding parameters, dimensions of elements and environmental conditions, the welded material, in particular HAZ, is subjected to cooling conditions. It determines the kinetics of structural changes in the solid state [50]. The possibility of predicting the effect of the thermal cycles of welding on the structure and weldability of the tested steel, in the case of underwater welding, is currently very difficult due to the lack of results of experimental tests and basic input data for numerical simulations. In this paper, the weldability assessment of underwater wet welding of S1300 steel by covered electrodes and with the use of TBW technique was investigated.

2. Materials and methods

For investigations, the S1300 UHSS steel was chosen. This material is characterized by fine-grained microstructures containing tempered martensite and bainite. Before welding, the chemical composition of S1300 steel was analyzed by spectrometry method. As a

Table 1
Chemical compositions of materials used (wt. %).

Material	C	Si	Mn	Ni	Cr	Cu	Mo	Al	Co	Ce_{IIW}[c]
S1300[a]	0.18	0.25	0.82	1.19	0.51	0.012	0.40	0.06	0.02	0.499
E42 2 1Ni RR 51 deposit[b]	0.05	0.45	0.50	0.03	–	–	–	–	–	0.133

[a] - in accordance with analysis.
[b] - in accordance with manufacturer data.
[c] - carbon equivalent as per International Institute of Welding.

filler, due to the lack of underwater electrodes for the investigated grade of steel, low carbon steel electrodes (4 mm diameter) for underwater applications were chosen. The electrode is comprised of a Si free C–Mn steel core wire with a thick rutile alumina silicate flux coating. It has a special formulated clear polymer based waterproof coating, to ensure the maximum resistance to water and moisture penetration. The nearest equivalent of filler material is E42 2 1Ni RR 51. The chemical compositions and mechanical properties of the used materials are presented in Tables 1 and 2. The mechanical properties of the electrodes were lower than the mechanical properties of the tested steel, which is a common practice when welding high-strength steel grades [27,31]. It resulted from lack of underwater covered electrodes ensure so high mechanical properties of deposited metal.

For experiment, the specimens with dimensions 4 × 80 × 160 mm and 10 × 80 × 160 mm have been prepared. They were used to access the influence of thickness on the effectiveness of the TBW technique. To evaluate the effectiveness of the TBW technique, the methodology consisting in performing two nonparallel beads was adopted [27], according to the scheme shown in Fig. 1. After finishing the first bead (tempered), the second (tempering) was laid on the surface of the plate to obtain different distances between the axes of the two beads (pitch). Between the two welds, the 120 s time was passed, following the procedure proposed in the previous investigations [27].

Welding process was carried out by MMA method. Specimens were welded at 0.5 m depth in tap water (20 °C). All specimens were welded with negative polarity (DC-) following the electrode manufacturer requirements. There are some investigations [51,52] which presented underwater wet welding with gravity systems. However, both the analysis of reports on underwater repair works in Europe and Asia, and the analysis of literature do not indicate the practical possibility of using automated MMA welding in non-laboratory conditions. To present the welding conditions closest to the real-life wet welding, in presented investigations the specimens were welded manually, by the underwater-welder with twenty years' experience. The welding stand is presented in Fig. 2.

During the preliminary test, different welding parameters were tested. For investigations the best were used, which allow to form weld beads with proper geometry assessed during visual test following requirements of EN ISO 17637:2017 standard [53]. The tempering beads were welded with a higher value of heat input (ql), to intensify the thermal tempering effect [27]. For test, two specimens were performed. Specimen A with 4 mm thickness and specimen B with 10 mm thickness. These specimens allow to achieve all ranges of pitch. The welding parameters are shown in Table 3.

Due to the expected high tendency of the tested steel to cold cracking, visual tests of the specimens were carried out after a delay time of 48 h in accordance with the guidelines of EN ISO 17637:2017 standard [53]. Each specimen was sampled with 0%, 50% and 100% pitch and prepared for further testing by standard techniques of mechanical cutting, grinding and polishing. Due to the fact that the welding process was carried out manually and the visibility of the underwater welding area was limited, it was difficult to obtain the initially assumed pitch values. Then the metallographic macro- and microscopic tests were conducted in accordance with EN ISO 17639:2013 [54] standard requirements. Each cross-section was etched by Vilella's reagent (ethanol 100 ml, hydrochloric acid 5 ml, picric acid 1 g). To determine the influence of the TBW on the microstructure and the number of cracks in different regions of underwater pad welds, microscopic observations were performed using the Olympus BX51 light microscope. The Vickers measurements were performed following the EN ISO 9015-1:2011 [55] standard with Sinowon V-10 hardness tester with a load of F = 98.07 N (HV10).

3. Results and discussion

3.1. Visual testing

During the process, typical problems for underwater wet welding were observed as gas bubbles and gas explosions above the water level, which lead to decreasing the visibility of the welded area [18,24]. However, no significant instability of the welding arc was observed during welding the specimen A. This allowed the specimen to be made in accordance with the welding procedure and scheme (Fig. 1). During visual testing of both specimens, no typical underwater imperfections such as cracks or undercuts were found in areas, from which the specimens for further investigations were taken. Near the beginning of the tempering bead in specimen B, small discontinuous were found (Fig. 3b, marked by red color). It was created during welding and resulted from a little instability of welding. However, this area was not considered for further investigations. The view of the surface of specimens is presented in Fig. 3. In the photos, the areas of cutting the specimens for further investigations were marked.

3.2. Macroscopic observations

The macrographs are presented in Fig. 4. None imperfections like pores and undercuts have been observed in the tested cross-sections. However, the crack was found in specimen B2 (Fig. 4d - marked by arrow), which was located in the HAZ of the first bead. Differences in specimens characterized by different thickness were found. The width of HAZ of 4 mm thick material is higher (Fig. 4a, c and 4e) in comparison to the 10 mm thick material (Fig. 4b, d and 4f). During welding with similar heat input values, the

Table 2
Mechanical properties of materials used following the manufacturer data.

Material	Minimum yield point, R_e (MPa)	Minimum tensile strength, R_m (MPa)	Minimum elongation, A_5 (%)
S1300	1300	1400	8
E42 2 1Ni RR 51 deposit	–	540	26

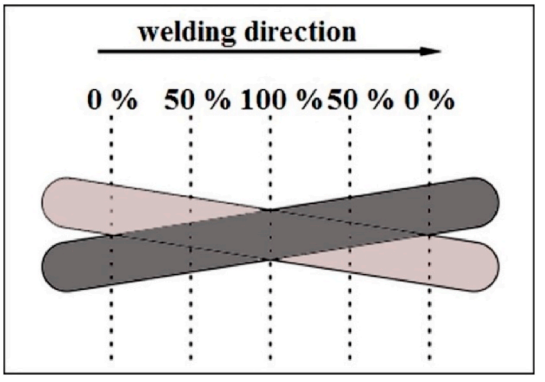

Fig. 1. The schematic view of TBW specimen. Dotted lines define pitch.

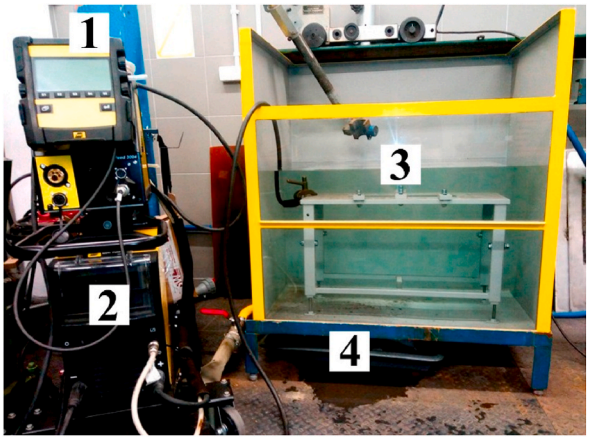

Fig. 2. The welding stand, 1 – Control panel, 2 – Welding power source, 3 – Welding table, 4 – Water tank.

Table 3
Welding parameters.

Specimen	Bead no.	Welding current, I (A)	Arc voltage, U (V)	Heat input, ql (kJ/mm)
A (thickness 4 mm)	1	204	24.8	4.8
	2	208	27.8	5.1
B (thickness 10 mm)	1	204	24.8	5.3
	2	208	28.3	5.4

heat is cumulated more in the thinner material, which provides to higher temperature of the metal due to differences in thermal severity. It leads to differences in the properties of the welded area, which was earlier proved by Yang et al. [56].

3.3. Microscopic observations

Investigated S1300 steel in delivery condition is characterized by a tempered martensite microstructure. During tests, the specimens were observed in different regions – especially in the weld metal and HAZ of the first (tempered) bead, which may show the influence of the heat from the second bead. The overview of pad welds are presented in Fig. 5. All pictures were taken along the axis of the first (tempered) bead. Microscopic tests showed differences of the weld metal and HAZ size between specimens characterized by different thickness. These differences were observed for each of the investigated pitches – 0%, 50% and 100%. Specimens with 4 mm thickness (Fig. 5a–c) are characterized by higher dimensions of weld metal and HAZ, which proved the results of the macroscopic test. The microscopic observations showed a typical microstructure of weld metal created in underwater wet welding conditions [19,20]. In each specimen, the dendritic microstructure consists of small-grained ferrite and the second phase in the column system was observed. For the specimens, in which the TBW was applied with pitch 0 or 50%, the second phase was bainite (Fig. 5a, b, 5e and 5f). Specimens which were performed with 100% pitch are characterized by the presence of tempered martensite as the second phase (Fig. 5c and e). These differences resulted from the influence of the heat from the tempering (second) bead. This effect was also observed in previous

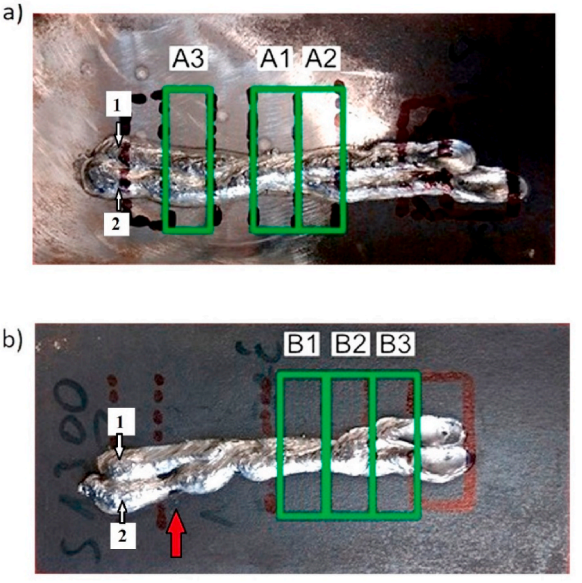

Fig. 3. View of specimens: a) specimen A (4 mm thickness), b) specimen B (10 mm thickness); 1 – tempered (first) bead, 2 – tempering (second) bead.

investigations for HSLA steels [27,31]. The application of TBW technique with short time (less than 120 s) affects the increasing the cooling time, which is crucial for the welded structures. It could resulted in the formation of a less brittle microstructure, which was proved for high-strength steels by Górka et al. [57]. As it was stated by Węglowski et al. [50], as the strength of steel increases, the structural uniformity increases. From this point of view, the presence of tempered martensite in the weld metal is desirable for S1300 steel wet welded structures. Also, the analysis of literature on the weldability of S1300 steel welded at different cooling rates shows that the structure of the joints is multi-phase and may contain MX precipitations, where M means V, Nb or Ti and X means C and N [58]. The impact of welding thermal cycles with the parameter to 2.5 s results in the formation of a martensitic structure with a hardness exceeding 450HV10. Extending the t8/5 cooling time to 60 s causes the formation of a martensitic-bainitic structure, while after extending the t8/5 cooling time over 60 s, a significant fraction by volume of ferrite was additionally found [58].

Microscopic overview showed cracks in different areas of the investigated specimens. The presence of cracks, especially in specimens without high influence of TBW was expected. S1300 UHSS steel is characterized by high value of carbon equivalent (Ce = 0.499%). The previous investigations [31] showed, that the number of cracks in underwater welded structures increased for steels with higher Ce value. The location and number of these cracks were investigated in the next step of the microscopic test. The exemplary micrographs of the cracks are presented in Fig. 6. For specimens A1 and B1 (both with pitch 0%), the welds consist of many short cracks near the axis of the bead (Fig. 6a and b). However, the smaller number was observed for thicker steel. Moreover, cracks were detected in the HAZ of both specimens with 0% pitch (Fig. 6c). These cracks are parallel to the fusion line (FL). The cracks parallel to FL located near the HAZ were also found in the weld metal of specimen B1 (Fig. 6d). Tomków et al. [27] proved that in underwater wet welding conditions, this type of cracks could be classified as cold cracks. For the specimens, in which the TBW was applied with the 50% pitch, the number of cracks decreased both in the weld (Fig. 6e and f) and in the HAZ (Fig. 6g and h). However, one big crack perpendicular to the FL was found in the HAZ in specimen B2 (Figs. 4d and 5e). This phenomenon could be explained by the statement from the literature. Tomków et al. [27] confirmed that TBW could not repair the microcracks that occurred during the welding of the first bead. In this case, the proposed technique could even lead to crack propagation. Specimens A3 and B3, which were welded with 100% beads overlapping, are characterized by the lowest number of cracks. In the weld, no cracks were found in the areas in which the second bead overlapped the first bead. Some short cracks, parallel to FL were found in regions near the fusion line in specimen A3, in which the two beads have not been overlapped (Fig. 6i). The same region in specimen B3 did not consist of any parallel cracks (Fig. 6j). However, one crack perpendicular to the FL was observed in this area (Fig. 5f). Different situation was observed in the HAZ of the specimens with 100% pitch. No cracks were observed in specimen B3 (Fig. 6l). In specimen A3, one perpendicular crack was observed near the axis of the weld (Fig. 5c). In the rest of HAZ, no cracks were found (Fig. 6k). Microscopic tests showed a small correlation between the number of cracks and the thickness of steel. In specimens with 4 mm thickness with the 0% and 50% pitch, a lower number of cracks were observed compared to 10 mm thickness specimens, with the same pitch. However, for 100% pitch, the number of cracks were greater in thicker steel than in sample with 4 mm thickness. As the percentage of beads overlapping increased, the overall number of cracks decreased, which was expected. Performed investigations proved that TBW leads to decreasing the number of cracks in the weld and in the HAZ of S1300 steel underwater welded structures. Vorkov et al. [59] proved that the high heat during bending leads to decreasing the susceptibility to cracking of S1300. Similar results were obtained in this research for welding processes. Covered electrodes used in the presented investigations generate 60–70 ml/100 g of diffusible hydrogen content in the deposited metal [18], which is one of the

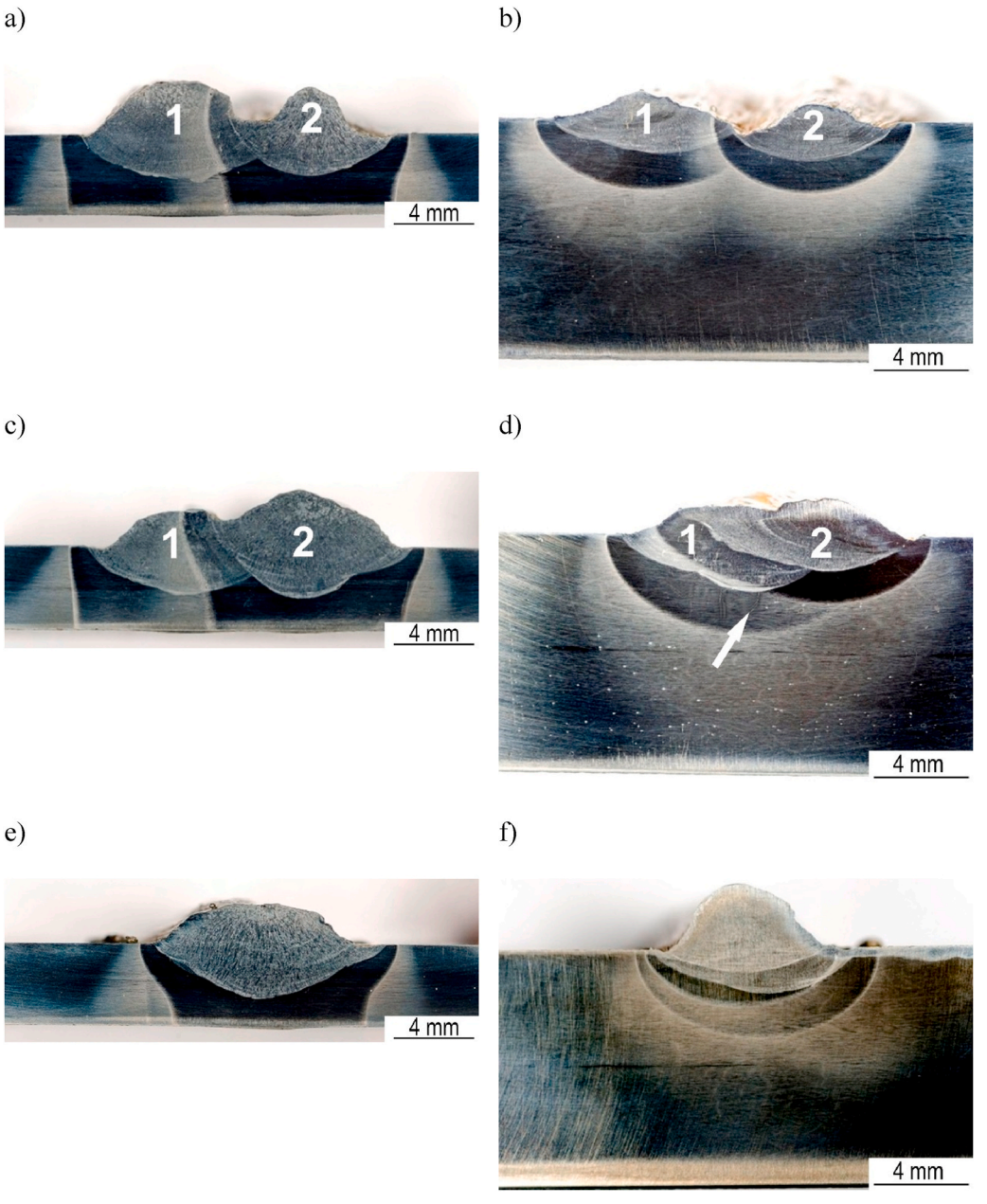

Fig. 4. The macrographs of: a) specimen A1, pitch 0%, b) specimen B1, pitch 0%, c) specimen A2, pitch 50%, d) specimen B2, pitch 50%, crack in the HAZ, e) specimen A3, pitch 100%, f) specimen B3, pitch 100%; 1 – first (tempered) bead, 2 – second (tempering) bead.

reasons of the observed cold cracks [60]. The proposed TBW technique allows to cumulate the heat in the metal, which resulted in the smaller number of cracks in the metal.

3.4. Hardness measurements

The distribution of hardness measurement points is presented in Fig. 7. Hardness was measured at five points in the line located in the axis of the first bead, perpendicular to the face of the weld. Three measurements were taken in the weld metal and three in the HAZ.

The results of hardness measurements are presented in Table 4. The comparison of the average values of hardness is shown in Fig. 8. Performed results allow to observe that the proposed TBW technique has a significant influence on the hardness of underwater welded structures performed on S1300 steel. This effect was observed both in specimens with 4 mm thickness and 10 mm thickness. The hardness of the weld metal decreased with increasing value of the pitch (Fig. 8a). These results were similar to the results of TBW application in S460 N steel [31]. In the presented article, the effect of the pitch on the significant reduction of the hardness of the weld

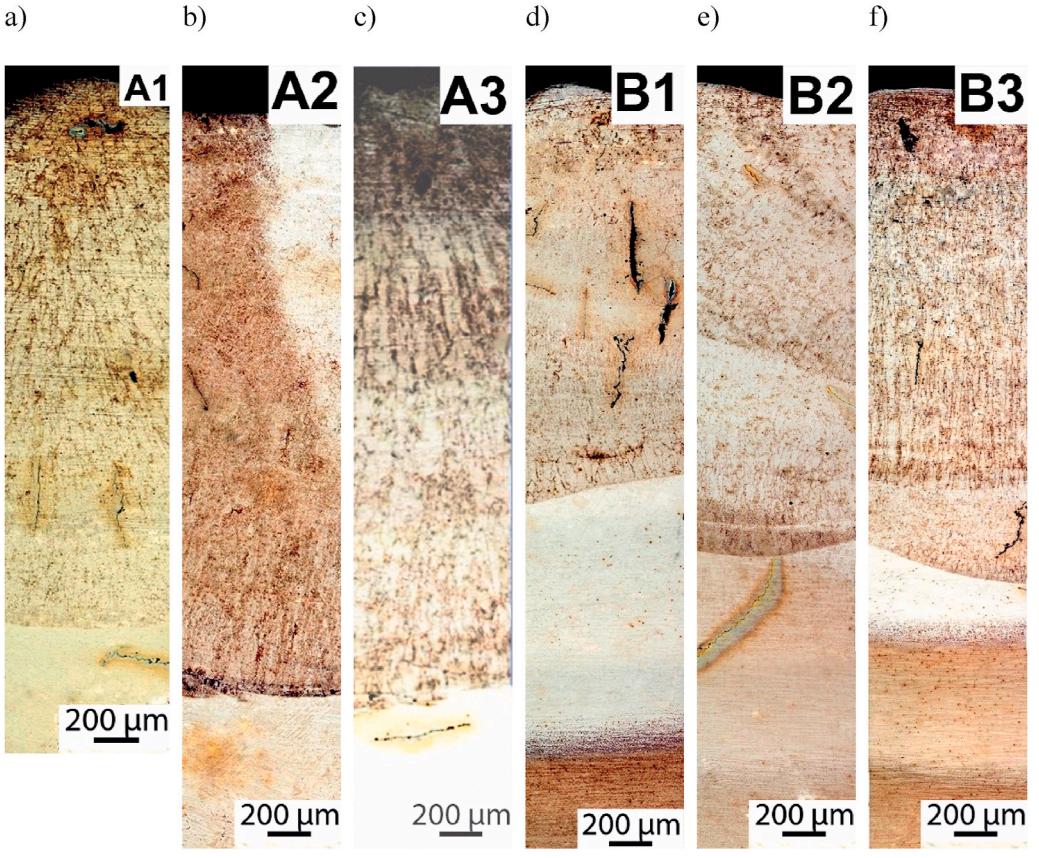

Fig. 5. The microscopic overview of: a) specimen A1, pitch 0%, b) specimen A2, pitch 50%, c) specimen A3, pitch 100%, d) specimen B1, pitch 0%, e) specimen B2, pitch 50%, f) specimen B3, pitch 100%.

metal has also been observed. However, as it was proved by Tomków et al. [27], the TBW has not affected the weld metal hardness in S355G10 + N steel joints. Results obtained in the present paper suggest that 100% pitch of TBW allows for the biggest reduction of the hardness in the HSLA and UHSS steel weld metal. Different correlation was observed in the HAZ (Fig. 8b). Additionally, in this region, the positive effect of TBW has been proved. However, the best results were observed for 50% pitch, both in specimen 4 mm thick and in specimen 10 mm thick. Most of the previous investigations in the field of TBW [27,31] showed that the best pitch in the reduction of the HAZ hardness is 100%. Tomków and Janeczek [61] tested the proposed technique during wet welding of S355J2C + N steel. They proved that welding with 100% pitch leads to increasing the hardness and did not affect the tempering of HAZ. Investigation of S1300 steel confirmed these results. It could be stated that the effect of the TBW application should be tested for each material. However, the proposed technique leads to decreasing the hardness in different regions of underwater welded structures. The investigated S1300 steel is classified into the material of group 3.2. in accordance with the EN ISO 15614-1:2017 standard [62]. Following its rules, the maximum hardness of HAZ should not exceed 450 HV10. The proposed TBW technique allows to fulfill the requirements of the mentioned standard. However, the hardness in HAZ of the underwater joints was higher than in the case of welding in air. Beniyash et al. [33] observed that HAZ of S1300 welded joint is characterized by hardness in the range of 320–380 HV10. Performed investigations showed the influence of material thickness on the HAZ hardness (Fig. 8b). Different thickness provide to the differences in the concentration of heat in both specimens. Different thermal severity resulted in differences of hardness in the HAZ after temper bead welding due to higher heat values near welding area. For specimen with bigger thickness, the heat value in welding area is smaller due to its transfer in whole (bigger) specimen. Moreover, it was found [63,64], that for advanced high-strength steels, the higher value of heat cumulated in the base metal resulted in decreasing the HAZ hardness, which was proved in presented paper.

4. Conclusions

In this paper, the novel study of the underwater wet welding of S1300 possibility has been investigated. It was proved that ultra-high strength steel could be used in the water environment for welded structures. Moreover, the usage of TBW technique has been positively verified.

The obtained results and their analysis allow to draw the following conclusions:

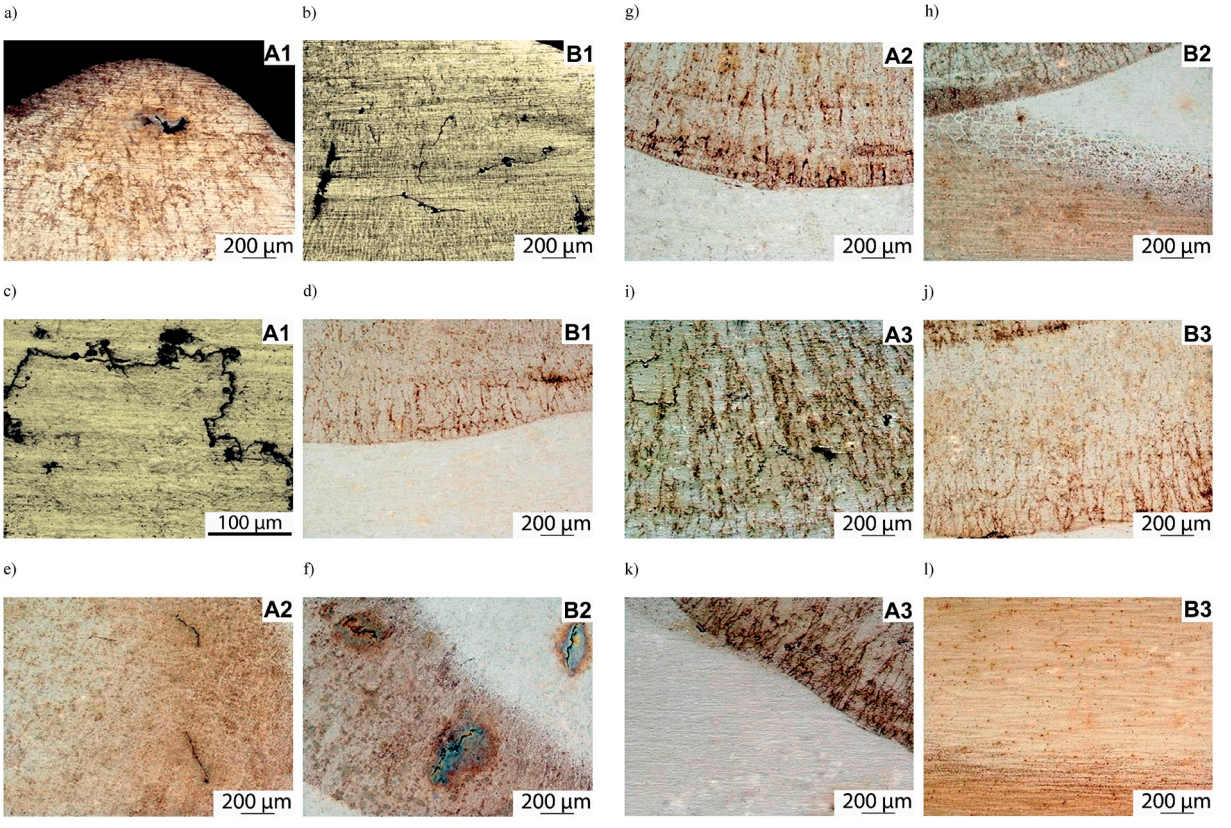

Fig. 6. Exemplary micrographs of: a) specimen A1, weld, pitch 0%, b) specimen B1, weld, pitch 0%, c) specimen A1, HAZ, pitch 0%, d) specimen B1, HAZ, pitch 0%, e) specimen A2, weld, pitch 50%, f) specimen B2, weld, pitch 50%, g) specimen A2, HAZ, pitch 50%, h) specimen B2, HAZ, pitch 50%, i) specimen A3, weld, pitch 100%, j) specimen B3, weld, pitch 100%, k) specimen A3, HAZ, pitch 100%, b) specimen B3, HAZ, pitch 100%.

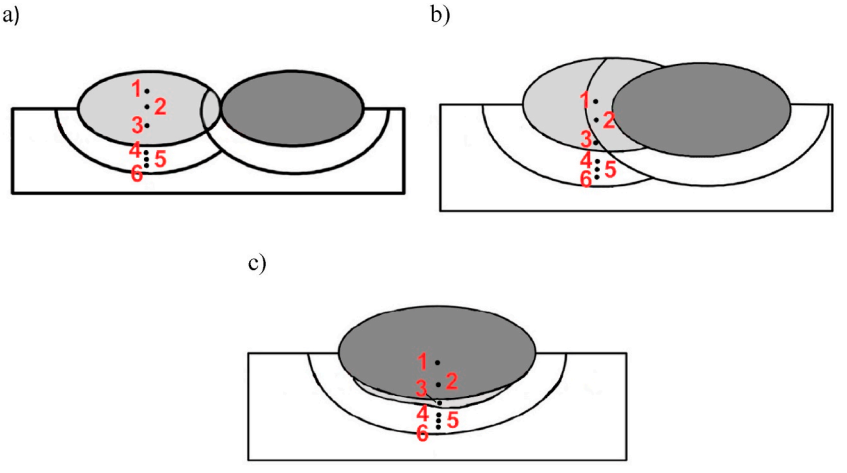

Fig. 7. Distribution of hardness measurement points: a) pitch 0%, b) pitch 50%, c) pitch 100%.

1. The investigated S1300 UHSS steel is characterized by high susceptibility to cold cracking in wet welding conditions. The weldability of the steel can be improved by application temper bead welding technique.
2. The TBW leads to decrease the number of cracks in the weld metal and in the HAZ in the tested specimens. The thickness of the welded material does not affect the effectiveness of the proposed technique. The number of cracks in the welds was lower in Specimen 1 (4 mm thick). However, the number of cracks in the HAZ was lower in the 10 mm thick specimen.

Table 4
Results of Vickers HV10 hardness measurements.

Specimen	Pitch, %	Base material	Measurement point					
			Weld metal			HAZ		
			1	2	3	4	5	6
A1	0	421	393	380	375	449	444	442
B1		432	403	417	393	525	482	490
A2	50	415	385	380	360	345	344	353
B2		412	382	364	372	485	443	437
A3	100	435	331	366	348	421	417	439
B3		427	331	317	329	472	502	501

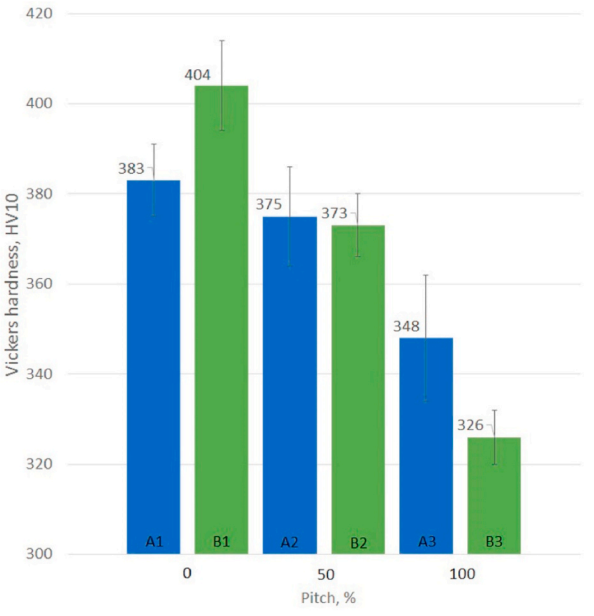

b)

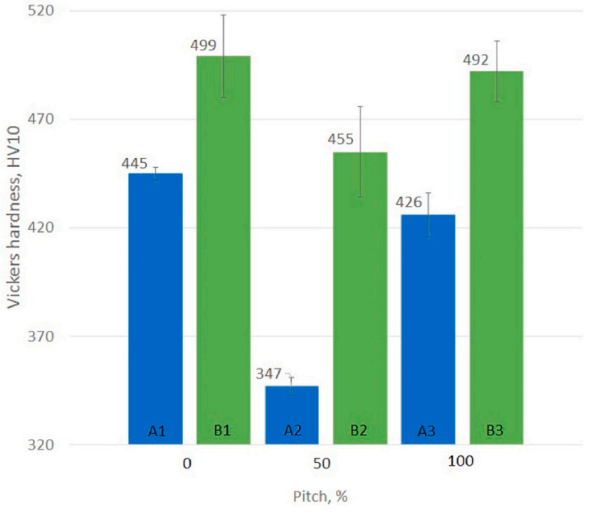

Fig. 8. Comparison of average values of hardness with different values of the pitch and standard deviation bars: a) in weld metal, b) in HAZ.

3. The hardness of the weld metal could be reduced by TBW technique. The decreasing of the hardness is strongly correlated with the increasing of the pitch. The 100% pitch allows to reduce the average hardness from 383 HV10 to 348 HV10 for 4 mm thick specimens. For the specimen with 10 mm thickness, the hardness decreased from 404 HV 10 to 326 HV 10.
4. Investigated TBW technique leads to decreasing the hardness in the HAZ of specimens with both used thickness. However, the greater decreasing was observed for 50% of beads' overlapping. The hardness was reduced from 445 HV10 to 347 HV10 in 4 mm thick specimens. Specimen with 10 mm thickness was characterized by a reduction of the hardness in the HAZ from 499 HV10 to 455 HV10.
5. From the point of view of the crack presence and the decreasing hardness in different regions of the welded joint, the best range of TBW pitch could be assessed as 50–100%. It allows to use the investigated S1300 UHSS steel for wet welded underwater structures.

Declaration of competing interest

The authors declare that they have no known competing financial interests or personal relationships that could have appeared to influence the work reported in this paper.

References

[1] Derazkola HA, Elyasi M. The influence of process parameters in friction stir welding of Al-Mg alloy and polycarbonate. J Manuf Process 2018;35:88–98. https://doi.org/10.1016/j.jmapro.2018.07.021.
[2] Golezani AS, Barenji RV, Heidarzadeh A, Pouraliakbar H. Elucidating of tool rotational speed in friction stir of 7020-T6 aluminum alloy. Int J Adv Manuf Technol 2015;81:1155–64. https://doi.org/10.1007/s00170-015-7252-6.
[3] Sajek A. Welding thermal cycles of joints made of S1100QL steel by saw and hybrid plasma-mag processes. Adv Mater Sci 2020;20:75–86. https://doi.org/10.2478/adms-2020-0023.
[4] Mičian M, Harmaniak D, Nový F, Winczek J, Moravec J, Trško L. Effect of the $t_{8/5}$ cooling time on the properties of S960MC steel in the HAZ of welded joints evaluated by thermal physical simulation. Metals 2020;10:229. https://doi.org/10.3390/met10020229.
[5] Çolak Z, Ayan Y, Kahraman N. Weld morphology and mechanical performance of marine structural steel welded underwater in a real marine environment. Int J Adv Manuf Technol 2020;109:491–501. https://doi.org/10.1007/s00170-020-05679-y.
[6] Parshin SG, Levchenko AM. Underwater hyperbaric dry welding of high strength steel arctic oil and gas pipeline. IOP Conf Ser: Earth Environ Sci 2020;539:012159. https://doi.org/10.1088/1755-1315/539/1/012159.
[7] Zhang X, Guo N, Xu C, Tan Y, Chen H, Zhang D. Flux cored arc welding of 304L stainless steel within glycerol environment. J Mater Process Technol 2020;283:116729. https://doi.org/10.1016/j.jmatprotec.2020.116729.
[8] Xu C, Guo N, Zhang X, Chen H, Fu Y, Zhou L. Internal characteristic of droplet and its influence on the underwater wet welding process stability. J Mater Process Technol 2020;280:116593. https://doi.org/10.1016/j.jmatprotec.2020.116593.
[9] Luo M, Wei P, Li Q, Hu R, Huang A, Pang S. Underwater laser welding of pure Ti: oxidation and hardening behaviors. Metals 2021;11:610. https://doi.org/10.3390/met11040610.
[10] Guo N, Fu Y, Xing X, Liu Y, Zhao S, Feng J. Underwater local dry cavity laser welding of 304 stainless steel. J Mater Process Technol 2020;260:146–55. https://doi.org/10.1016/j.jmatprotec.2018.05.025.
[11] Han L, Jiang D, Xu M, Zhang Q, Wang Z. Effect of gas pressure on the formation mechanism of welds based on local dry underwater welding. ISIJ Int 2021;61:317–25. https://doi.org/10.2355/isijinternational.ISIJINT-2020-231.
[12] Tomków J, Janeczek A, Rogalski G, Wolski A. Underwater local cavity welding of S460N steel. Materials 2020;13:5535. https://doi.org/10.3390/ma13235535.
[13] Bunaziv I, Aune R, Olden V, Akselsen OM. Dry hyperbaric welding of HSLA steel up to 35 bar ambient pressure with CMT arc mode. Int J Adv Manuf Technol 2019;105:2659–76. https://doi.org/10.1007/s00170-019-04511-6.
[14] Gheonea MC, Florescu SN, Mihailescu D, Teodor V. Influence of marine corrosion on the roughness of dry hyperbaric underwater MAG welding joints. IOP Conf Ser: Mater Sci Eng 2020;968:012009.
[15] Wang J, Sun Q, Zhang T, Tao X, Jin P, Feng J. Arc stability indexes evaluation of ultrasonic wave-assisted underwater FCAW using electrical signal analysis. Int J Adv Manuf Technol 2019;103:2593–608. https://doi.org/10.1007/s00170-019-03463-1.
[16] Chen H, Guo N, Xu K, Liu C, Wang G. Investigating the advantages of ultrasonic-assisted welding technique applied in underwater wet welding by in-situ X-ray imaging method. Materials 2020;13:1442. https://doi.org/10.3390/ma13061442.
[17] Wu J, Han Y, Jia C, Wu C, Yang Q. Underwater pulse-current FCAW – Part 2: bubble behaviors and waveform optimization. Weld J 2020;99:303–11. https://doi.org/10.29391/2020.99.028.
[18] Tomków J, Fydrych D, Wilk K. Effect of electrode waterproof coating on quality of underwater wet welded joints. Materials 2020;13:2947. https://doi.org/10.3390/ma13132947.
[19] Moreno-Uribe AM, Bracarense AQ, Pessoa ECP. The effect of polarity and hydrostatic pressure on operational characteristics of rutile electrode in underwater welding. Materials 2020;13:5001. https://doi.org/10.3390/ma13215001.
[20] Wang J, Ma J, Liu Y, Zhang T, Wu S, Sun Q. Influence of heat input on microstructure and corrosion resistance of underwater wet-welded E40 steel joints. J Mater Eng Perform 2020;29:6987–96. https://doi.org/10.1007/s11665-020-05160-7.
[21] Parshin SG, Levchenko AM, Maystro AS. Metallurgical model of diffusible hydrogen and non-metallic slag inclusions in underwater wet welding of high-strength steel. Metals 2020;10:1498. https://doi.org/10.3390/met10111498.
[22] Fydrych D, Łabanowski J. An experimental study of high-hydrogen welding processes. Rev Metal 2015;51:e055. https://doi.org/10.3989/revmetalm.055.
[23] Tomków J, Fydrych D, Rogalski G, Łabanowski J. Effect of the welding environment and storage time of electrodes on the diffusible hydrogen content in deposited metal. Rev Metal 2019;55:e140. https://doi.org/10.3989/revmetalm.140.
[24] Klett J, Hecht-Linowitzki V, Grünzel O, Schmidt E, Maier HJ, Hassel T. Effect of the water depth on the hydrogen content in SMAW wet welded joints. SN Appl. Sci. 2020;2:1269. https://doi.org/10.1007/s42452-020-3066-8.
[25] Fydrych D, Świerczyńska A, Tomków J. Diffusible hydrogen control in flux cored arc welding process. Key Eng Mater 2013;597:171–8. https://dx.doi.org/10.4028/www.scientific.net/KEM.597.171.
[26] Klett J, Hassel T. Influence of stick electrode coating's moisture content on the diffusible hydrogen in underwater wet shielded metal arc welding. Adv Mater Sci 2020;20:27–37. https://doi.org/10.2478/adms-2020-0020.
[27] Tomków J, Rogalski G, Fydrych D, Łabanowski J. Improvement of S355G10+N steel weldability in water environment by Temper Bead Welding. J Mater Process Technol 2018;262:372–81. https://doi.org/10.1016/j.jmatprotec.2018.06.034.
[28] Kumar S, Kumar S, Pandey C, Goyal A. Effect of post-weld heat treatment and dissimilar filler metal composition on the microstructural developments, and mechanical properties of gas tungsten arc welded joint of P91 steel. Int J Pres Ves Pip 2021;191:104373. https://doi.org/10.1016/j.ijpvp.2021.104373.
[29] Surojo E, Anindito J, Paundra F, Prabowo AR, Budiana EP, Muhayat N, Badaruddin M, Triyono. Effect of water flow and depth on fatigue crack growth rate of underwater wet welded low carbon steel SS400. Open Eng 2021;11:329–38. https://doi.org/10.1515/eng-2021-0036.

[30] Tomków J. Weldability of underwater wet welded HSLA steel: effect of electrode hydrophobic coating. Materials 2021;14:1364. https://doi.org/10.3390/ma14061364.
[31] Tomków J, Fydrych D, Rogalski G. Dissimilar underwater wet welding of HSLA steels. Int J Adv Manuf Technol 2020;109:717–25. https://doi.org/10.1007/s00170-020-05617-y.
[32] Sun K, Hu Y, Shi Y, Liao B. Microstructure evolution and mechanical properties of underwater dry welded metal of high strength steel Q690E under different water depths. Pol Marit Res 2020;27:112–9. https://doi.org/10.2478/pomr-2020-0071.
[33] Beniyash A, Klimov G, Hassel T. The use of non-vacuum electron beam (NVEB) technology as an universal manufacturing process for welding and cutting of high-strength steels. J Phys: Conf Ser 2018;1089:012012. https://doi.org/10.1088/1742-6596/1089/1/012012.
[34] Ning J, Zhang LJ, Yang JN, Yin QX, Wang XW, Wu J. Characteristics of multi-pass narrow-gap laser welding of D406A ultra-high strength steel. J Mater Process Technol 2019;270:168–81. https://doi.org/10.1016/j.jmatprotec.2019.02.026.
[35] Gao W, Wang D, Cheng F, Deng C, Liu Y, Xu W. Enhancement of the fatigue strength of underwater wet welds by grinding and ultrasonic impact treatment. J Mater Process Technol 2015;223:305–12. https://doi.org/10.1016/j.jmatprotec.2015.04.013.
[36] van Es S, Slot H, Steenbergen H, Maljaars J, Pijpers R. Use of HSS and VHSS in steel structures in civil and offshore engineering. Steel Constr 2018;11:249–56. https://doi.org/10.1002/stco.201800018.
[37] Berg J, Stranghoener N. Fatigue strength of welded ultra high strength steels improved by high frequency hammer peening. Procedia Mater. Sci. 2014;3:71–6. https://doi.org/10.1016/j.mspro.2014.06.015.
[38] Shiozaki T, Yamaguchi N, Tamai T, Hiramoto J, Ogawa K. Effect of weld toe geometry on fatigue life of lap fillet welded ultra-high strength steel joint. Int J Fatig 2018;116:409–20. https://doi.org/10.1016/j.ijfatigue.2018.06.050.
[39] Ahola A, Muikku A, Braun M, Björk T. Fatigue strength assessment of ground filler-welded joints using 4R method. Int J Fatig 2021;142:105916. https://doi.org/10.1016/j.ijfatigue.2020.105916.
[40] Mecséri BJ, Kövesdi B. Assessment of grinding weld treatment methods using effective notch stresses. Weld World 2020;64:1033–46. https://doi.org/10.1007/s40194-020-00894-3.
[41] Braun M, Wang X. A review of fatigue test data on weld toe grinding and weld profiling. Int J Fatig 2021;145:106073. https://doi.org/10.1016/j.ijfatigue.2020.106073.
[42] Schaupp T, Rhode M, Yahyaoui H, Kannengiesser T. Hydrogen-assisted cracking in GMA welding of high-strength structural steels using the modified spray arc process. Weld World 2020;64:1997–2009. https://doi.org/10.1007/s40194-020-00978-0.
[43] Ottersböck MJ, Leitner M, Stoschka M, Maurer W. Crack initiation and propagation fatigue life of ultra high-strength steel butt joints. Appl Sci 2019;9:4590. https://doi.org/10.3390/app9214590.
[44] Amraei M, Ahola A, Afkhami S, Björk T, Haidarpour A, Zha XL. Effects of heat input on the mechanical properties of butt-welded high and ultra-high strength steels. Eng Struct 2019;198:109460. https://doi.org/10.1016/j.engstruct.2019.109460.
[45] Schaffner T, Hartmaier A, Kokotin V, Pohl M. Analysis of hydrogen diffusion and trapping in ultra-high strength steel grades. J Alloys Compd 2018;746:557–66. https://doi.org/10.1016/j.jallcom.2018.02.264.
[46] Lim MK, Ha SS. Ultra-high-strength grout for filling steel pipe in offshore wind turbines. Int J Appl Eng Res 2017;23:13064–76.
[47] Xi X, Li S, Yang S, Li J, Zhao M. Effect of adding yttrium on precipitation behaviors of inclusions in E690 ultra high strength offshore platform steel. High Temp Mater Process 2020;39:510–9. https://doi.org/10.1515/htmp-2020-0089.
[48] Herion S. The properties of steels used in jack-up platforms. In: Carlton J, Jukes P, Choo YS, editors. Encyclopedia of maritime and offshore engineering. New York: Wiley; 2018. p. 1–16.
[49] Braun M, Kahl A, Willems T, Seidel S, Fischer C, Ehlers S. Guidance for material selection based on static and dynamic mechanical properties at sub-zero temperatures. J Offshore Mech Arctic Eng 2021;143:1–45. https://doi.org/10.1115/1.4049252.
[50] Węglowski MS, Zeman M, Łomozik M. Physical simulation of weldability of Weldox 1300 steel. Mater Sci Forum 2013;792:551–5. https://dx.doi.org/10.4028/www.scientific.net/MSF.762.551.
[51] Arias AR, Bracarense AQ. Fatigue crack growth assessment in underwater wet welds. Weld J 2017;96:287–94.
[52] Menezes PHR, Pessoa ECP, Bracarense AQ. Comparison of underwater wet welding performed with silicate and polymer agglomerated electrodes. J Mater Process Technol 2019;266:63–72. https://doi.org/10.1016/j.jmatprotec.2018.10.019.
[53] EN ISO 17637. Non-destructive testing of welds—visual testing of fusion-welded joints. 2017.
[54] EN ISO 17639. Destructive tests on welds in metallic materials. In: Macroscopic and microscopic examination on welds; 2013.
[55] EN ISO 9015-1. Destructive tests on welds in metallic materials. In: Hardness testing. Hardness test on arc welded joint; 2011.
[56] Yang X, Di X, Liu X, Wang D, Li C. Effects of heat input on microstructure and fracture toughness of simulated coarse-grained heat affected zone for HSLA steels. Mater Char 2019;155:109818. https://doi.org/10.1016/j.matchar.2019.109818.
[57] Górka J, Janicki D, Fidali M, Jamrozik W. Thermographic assessment of the HAZ properties and structure of thermomechanically treated steel. Int J Thermophys 2017;38:183. https://doi.org/10.1007/s10765-017-2320-9.
[58] Węglowski M, Zeman M, Grocholewski A. Effect of welding thermal cycles on microstructure and mechanical properties of simulated heat affected zone for a Weldox 1300 ultra-high strength alloy steel. Arch Metall Mater 2016;61:127–32. https://doi.org/10.1515/amm-2016-0024.
[59] Vorkov V, Garcia AT, Duflou JR. Bending parameters in heat assisted air bending of high strength steels. Procedia Manuf 2020;47:1314–8. https://doi.org/10.1016/j.promfg.2020.04.250.
[60] Węgrzyn T, Symczak T, Szczucka-Lasota B, Łazarz B. MAG welding process with micro-jet cooling as effective method for manufacturing joints for S700MC steel. Metals 2021;11:276. https://doi.org/10.3390/met11020276.
[61] Tomków J, Janeczek A. Underwater in situ local heat treatment by additional stitches for improving the weldability of steel. Appl Sci 2020;10:1823. https://doi.org/10.3390/app10051823.
[62] EN ISO 15614-1. Specification and qualification of welding procedures for metallic materials—welding procedure test—Part 1: arc and gas welding of steels and arc welding of nickel and nickel alloys. 2017.
[63] Tomków J, Świerczyńska A, Landowski M, Wolski A, Rogalski G. Bead-on-plate underwater wet welding on S700MC steel. Adv Sci Technol Res J 2021;15(3):288–96. https://doi.org/10.12913/22998624/140223.
[64] Tomków J, Landowski M, Rogalski G. Application possibilities of the S960 steel in underwater welded structures. Facta Univ Ser: Mech Eng 2022. In press.